Scanning Auger Microprobe Qualitative Analysis

Si C in AL Alloy 2124

Langley Sample No. A623524

Prepared by: R. Browning

NASA-Ames Research Center

Moffett Field, CA 94035

(415) 965-5550

(NASA-TM-89623) SCANNING AUGER MICROPROBE QUALITATIVE ANALYSIS SiC IN Al ALLOY 2124, LANGLEY SAMPLE NO. A623524 (NASA) 38 p
Avail: NTIS

N87-70431

Unclas
00/25 0079392

Scanning Auger Microprobe Qualitative Analysis

Langley Sample A6235Z4

Given system: SiC reinforced Al alloy.

Alloy 2124

	Al	Cu	Mn	Mg
by Wht.	93.5	4.4	0.6	1.5

The sample was cut and polished in the direction of the extrusion.

SEM appearance: Fig. 1 shows a typical region of this sample. There is sufficient relief in the surface to see clearly the SiC fibres and other features. The axes of the SiC fibres appear to be distributed fairly randomly around the surface normal. There is a large variation in the size of the fibres.

Auger analysis: Fig. 2 shows some of the typical points of interest of Fig. 1. Fig. 3 is an Auger spectrum of the whole of this region and shows that the major features are Al, Si, C and O. Point A in the center of the micrograph is a flat region shown at a higher magnification in Fig. 4. Fig. 5 is the similar region D. The Auger spectrum from these regions is shown in Fig. 6. This spectrum shows that the features are Mg/Al with small amounts of C and O which are probably surface contaminants. Some Si appears to be present but Cu and Mg are low to undetectable. Point B in the middle right of the micrograph Fig. 2 is shown at higher magnification in Fig. 7. The Auger spectrum from this feature shows it to be a large SiC fibre near normal to the surface. Fig. 9 is an enlargement of the fibre/matrix boundary region on the left hand side of the fibre. The

bright dotted line shows the position of an Auger line scan taken across this boundary. The length of this line is 1.2_u. The multiple Auger line scan Fig. 10 is of Al 68eV, Si 90eV, C 264eV and O 500eV. The line scan shows that there is an Al oxide region ~1_u wide between the Al matrix and the SiC particle. This result might be significant but should be treated cautiously. The topographic relief of the sample may cause some shadowing of the Argon ion beam used for cleaning the sample. However, the spectrum from this region is very similar to that of point E which is certainly an Al_2O_3 particle because of its charging at low SEM voltages. This region and the spectrum are shown in Fig. 11 and 12. There are also MgO particles which similarly charge at low SEM voltages. The stability of the beam position over the acquisition time (5 mins) is not sufficient to discriminate against signal from adjacent regions but the spectrum does show that there is no detectable accumulation of Cu, Mn, or Mg at this boundary. Point C in the lower left hand side of micrograph Fig. 2 is shown at greater magnification in Fig. 13. This is a flat region and from the Auger spectrum in Fig. 12 is a Cu/Al alloy. Point F is shown enlarged in Fig. 15 and is a typical matrix region. The Auger spectrum is shown in Fig. 16. This indicates merely that the matrix is greater than 90% Al. Note that the low energy tail of the Auger transition is much less than that of Fig. 12 showing that the oxygen is just a surface contaminant.

Conclusion: The sample has a very inhomogeneous distribution of constituents. The minor constituents of the nominal Al alloy are not detected in the typical matrix, but are found in distinct regions. The Cu, Mn are segregated into 1-10u sized particles that are binary Al alloys. The Mg also segregates, but into smaller particles that are MgO. A boundary region between one SiC fiber and the matrix was found and this region is Al_2O_3.

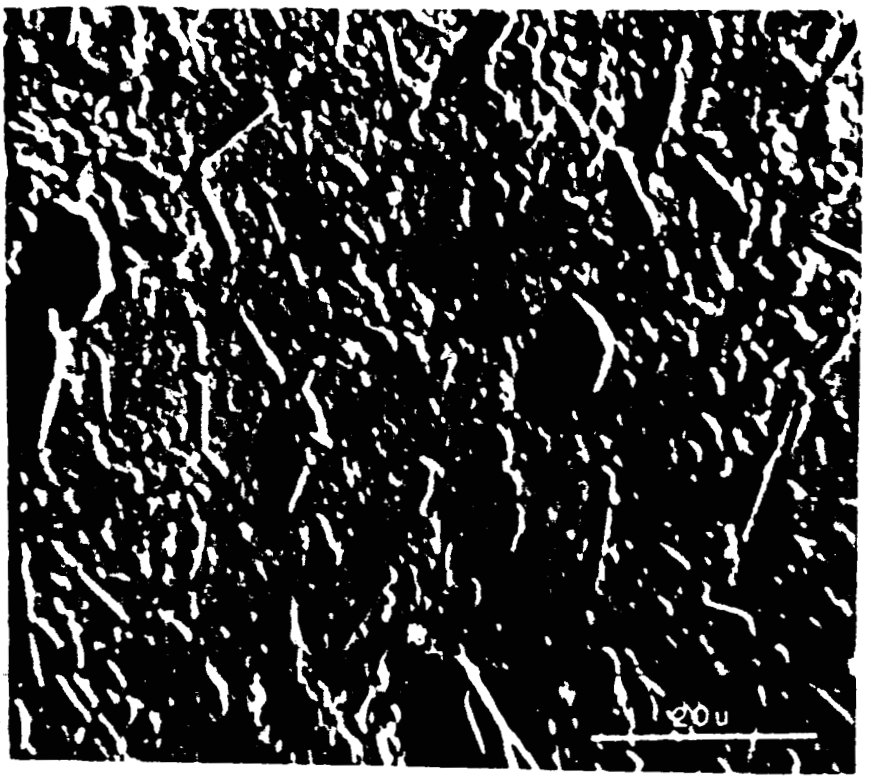

FIG 1

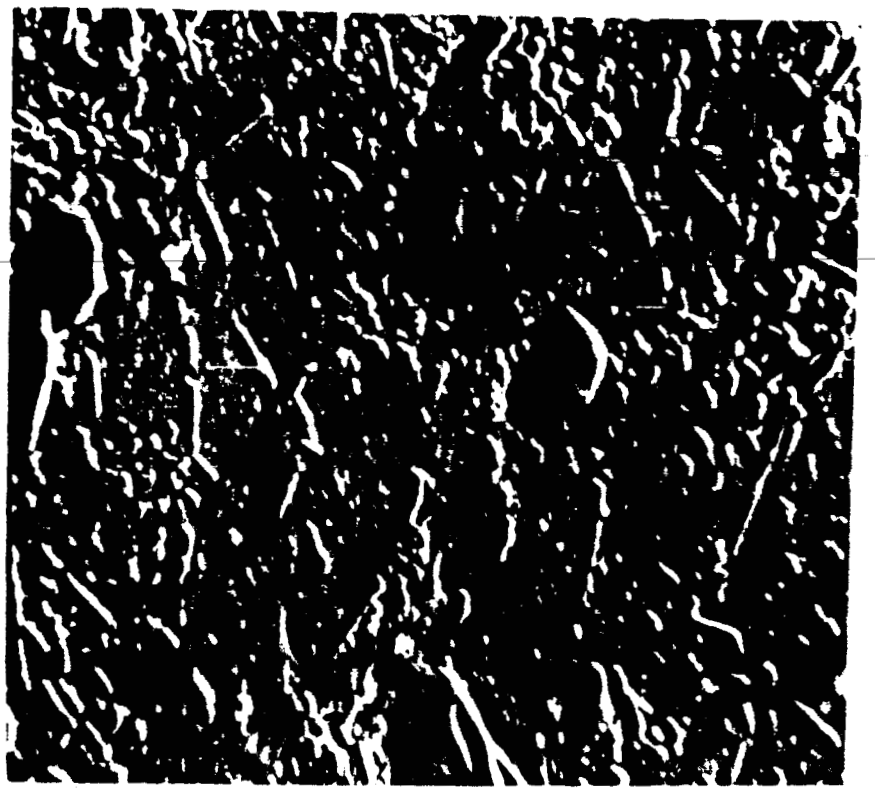

FIG 2

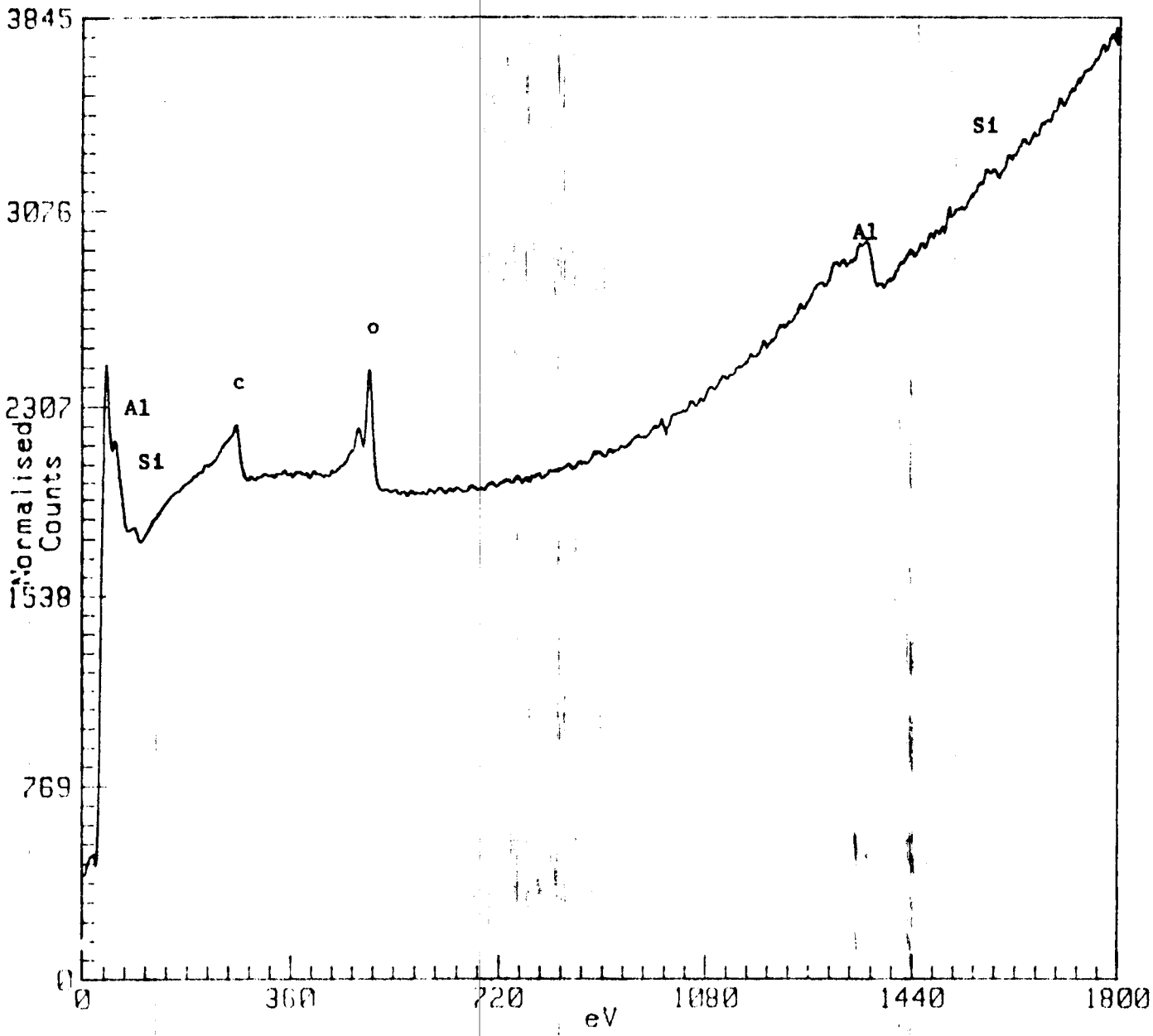

FIG 3

Spectrum from area of Fig 1.

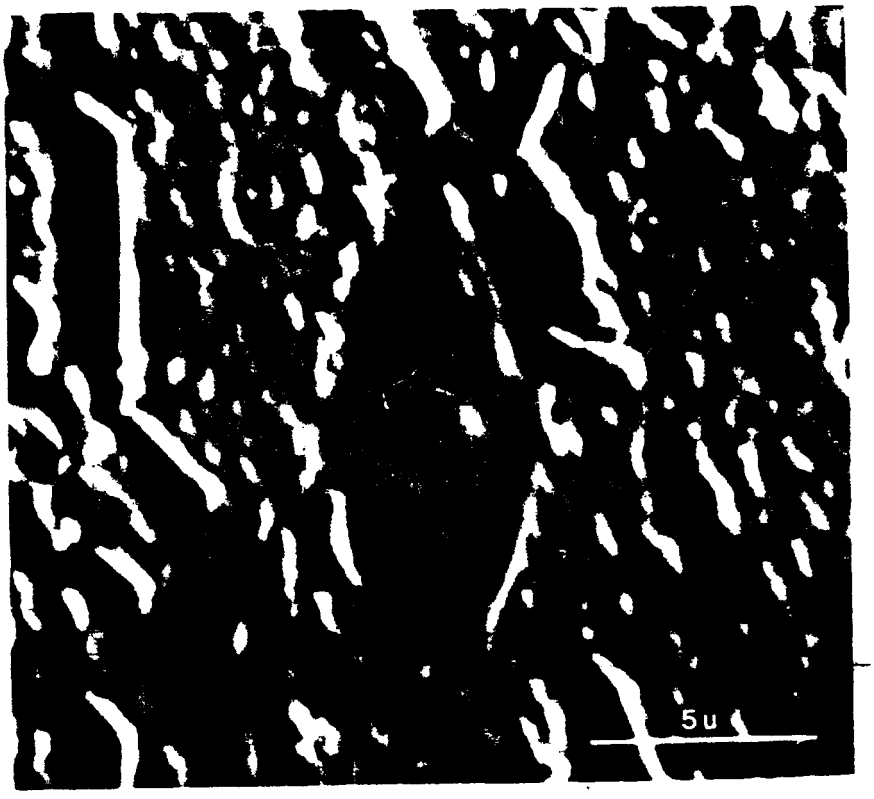

FIG 4

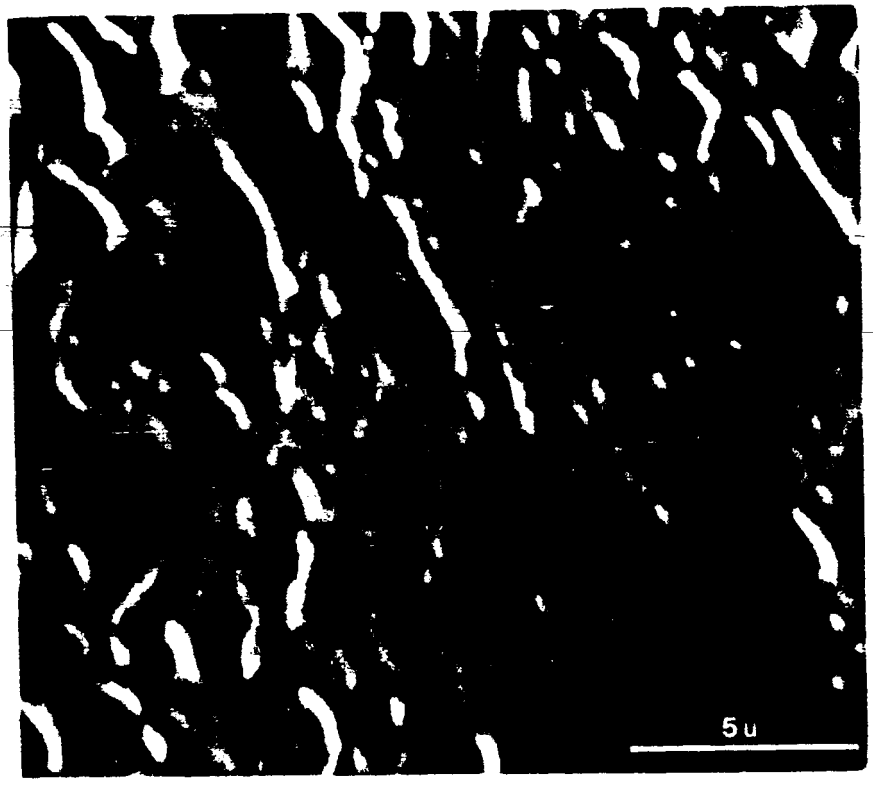

FIG 5

Mn/Al regions , spectrum Fig 6.

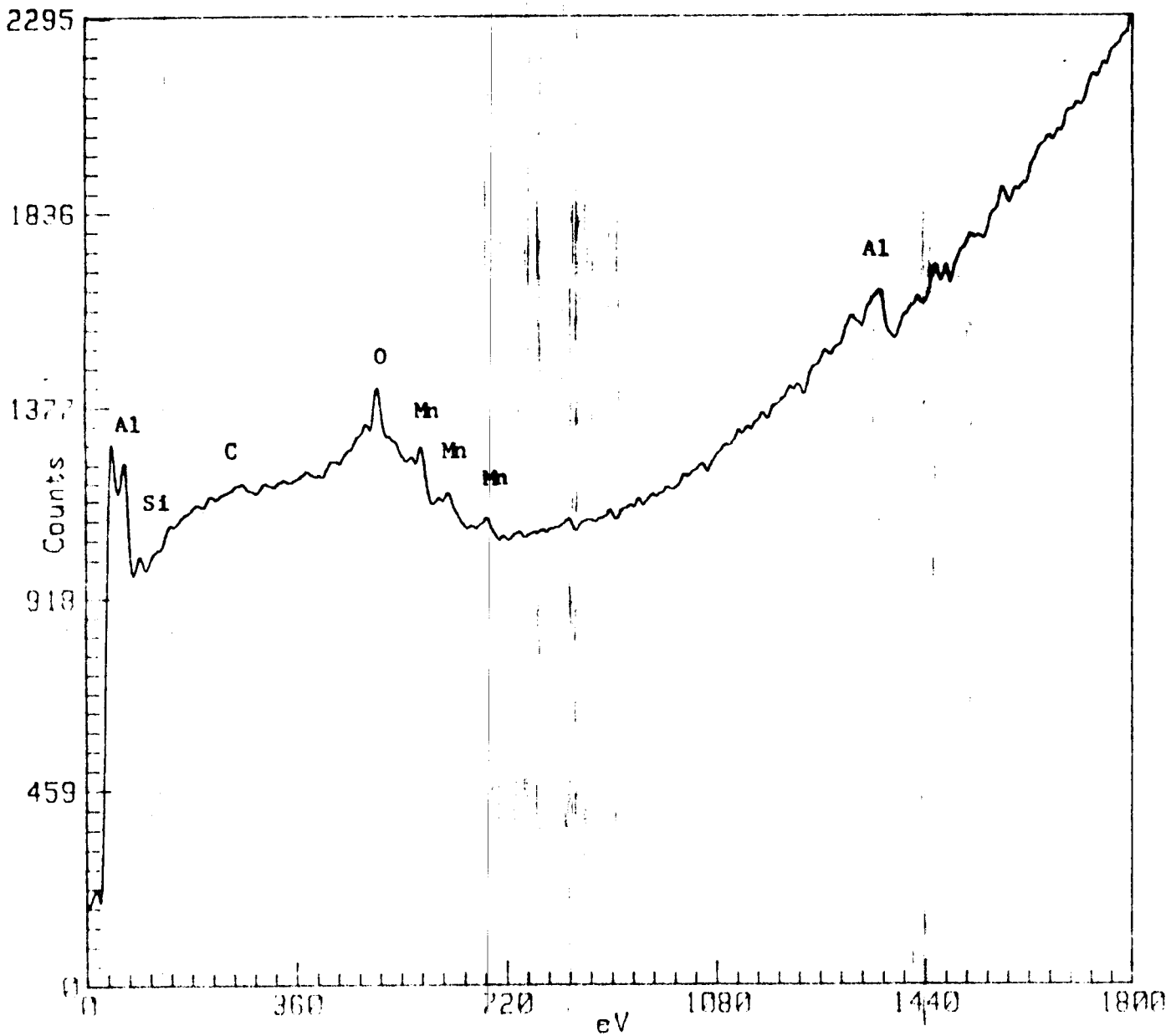

FIG 6

spectrum ofpoints A and D

Large SiC particle

FIG 7

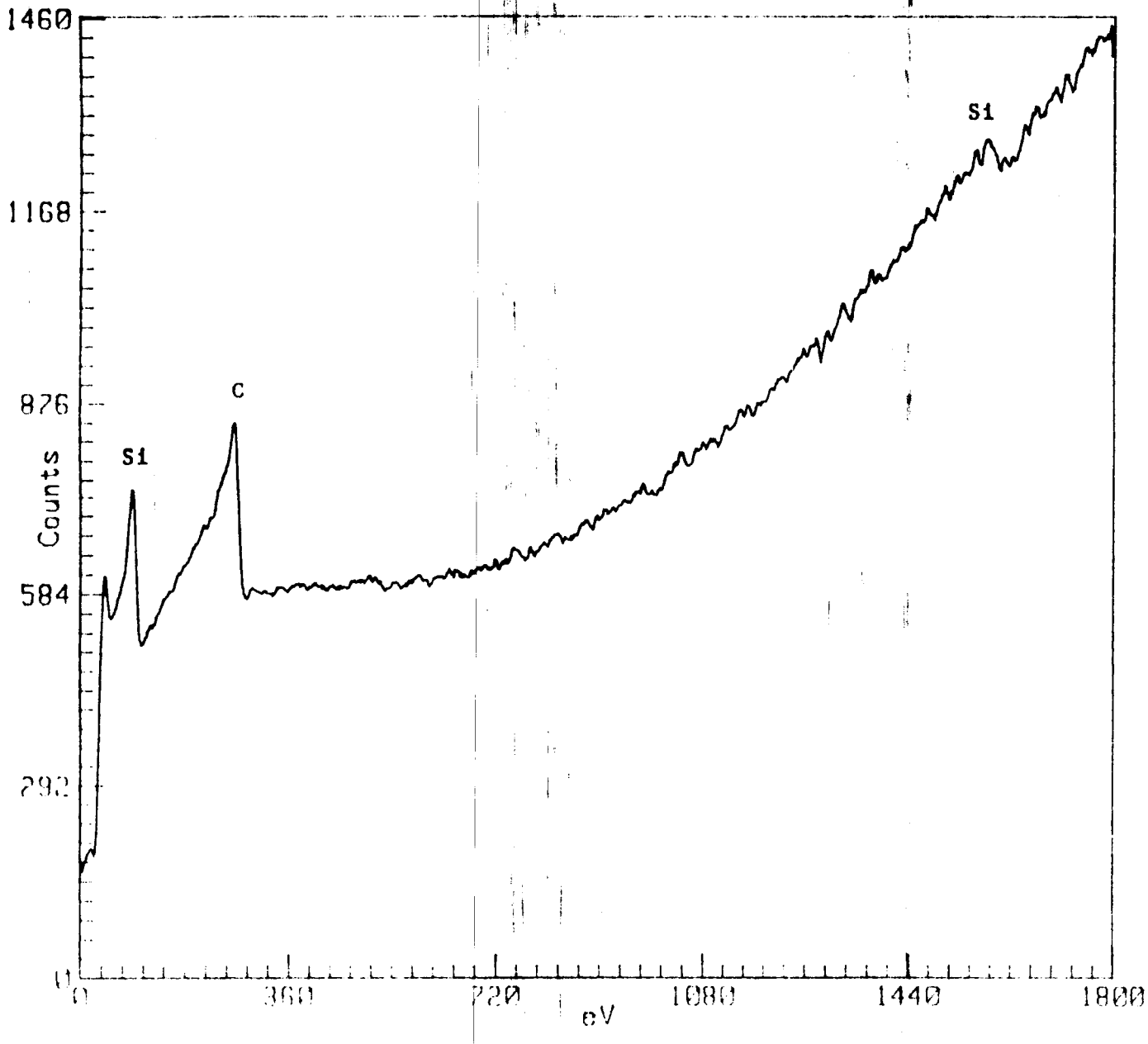

FIG 8

Spectrum of particle in fig 7, Si6

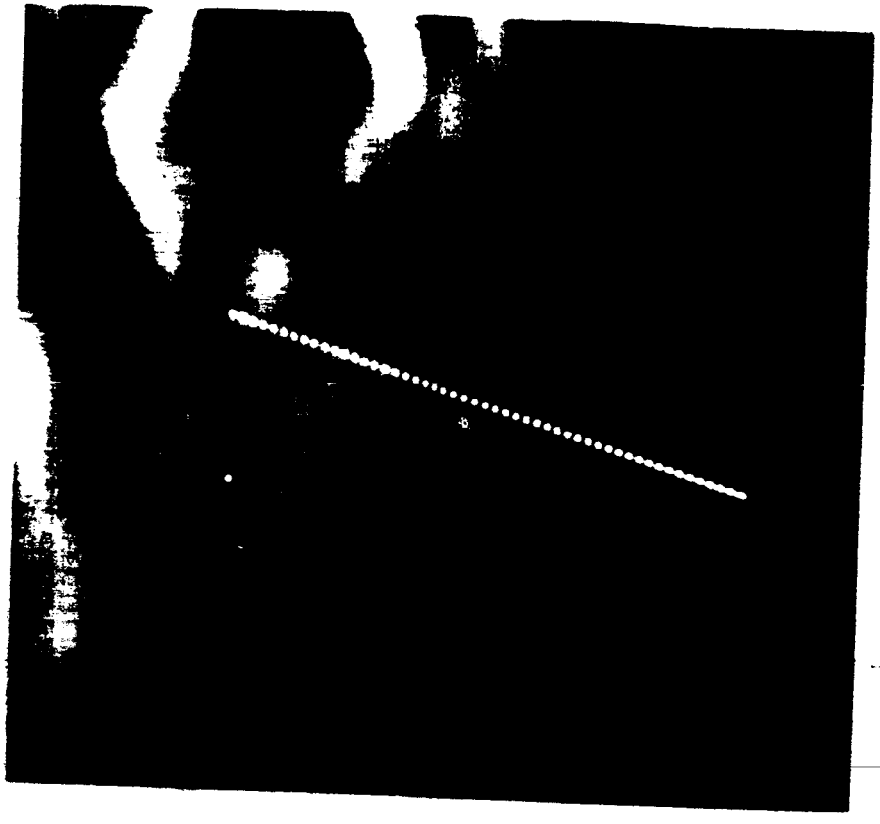

Al/SiC boundary.

FIG 9

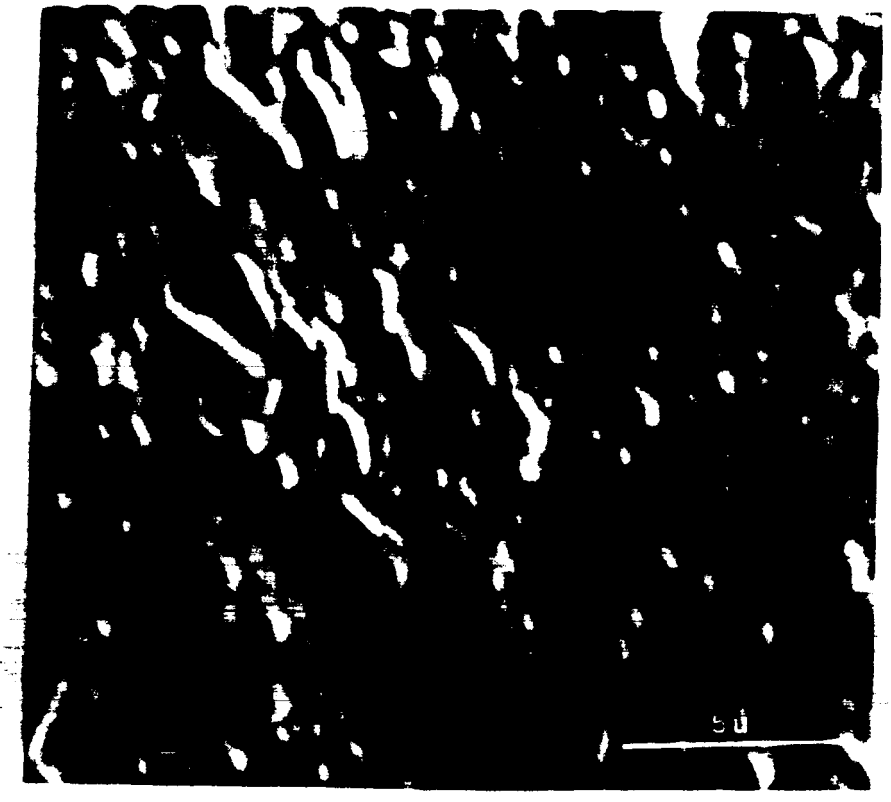

Point E

FIG 11

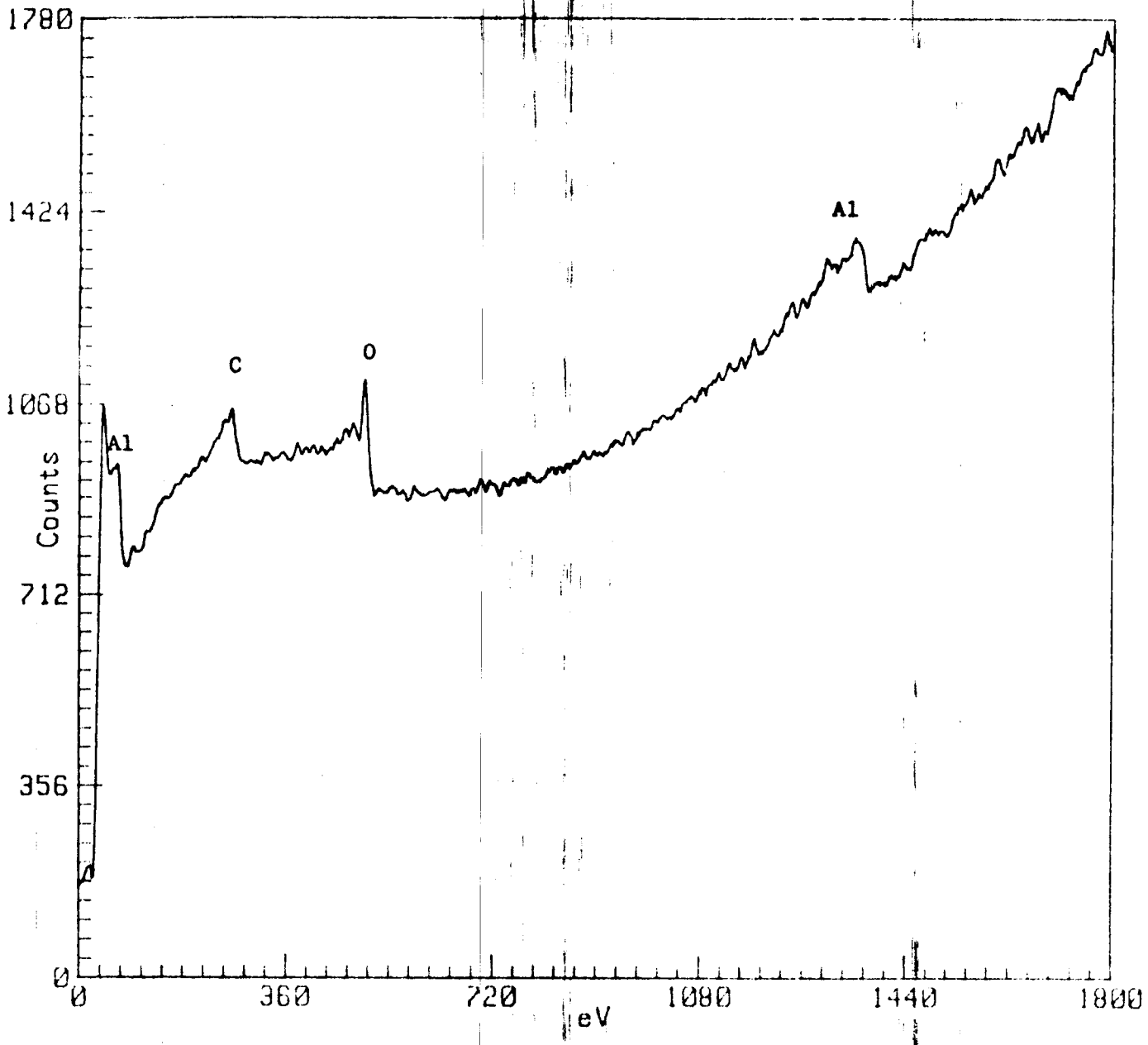

FIG 12

Spectrum of point E and Al/SiC boundary.

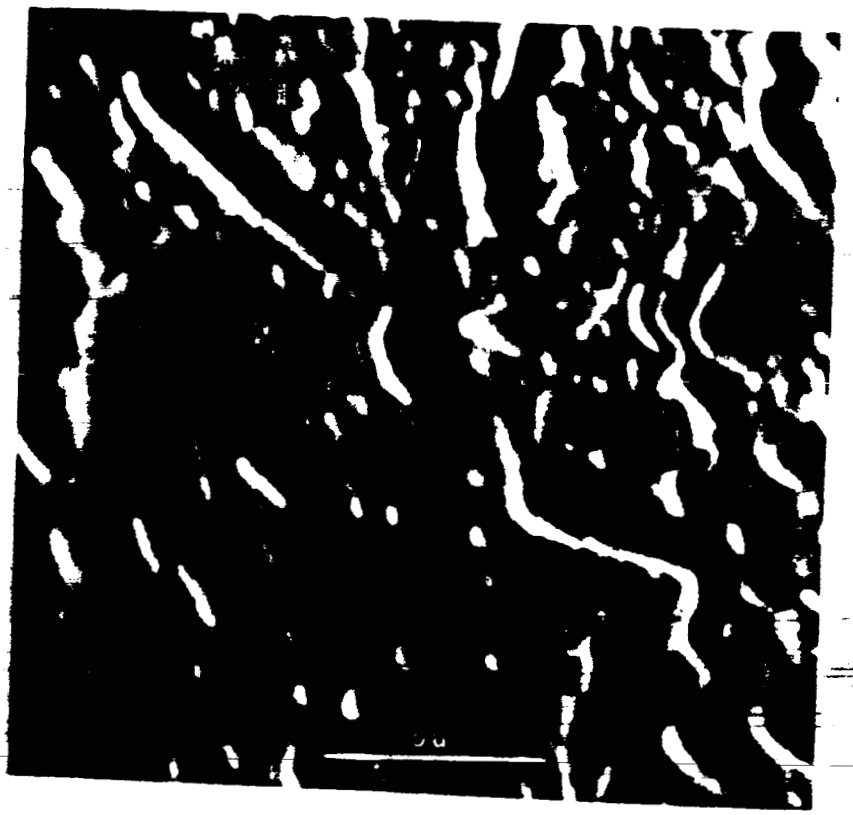

Cu/Al region

FIG 13

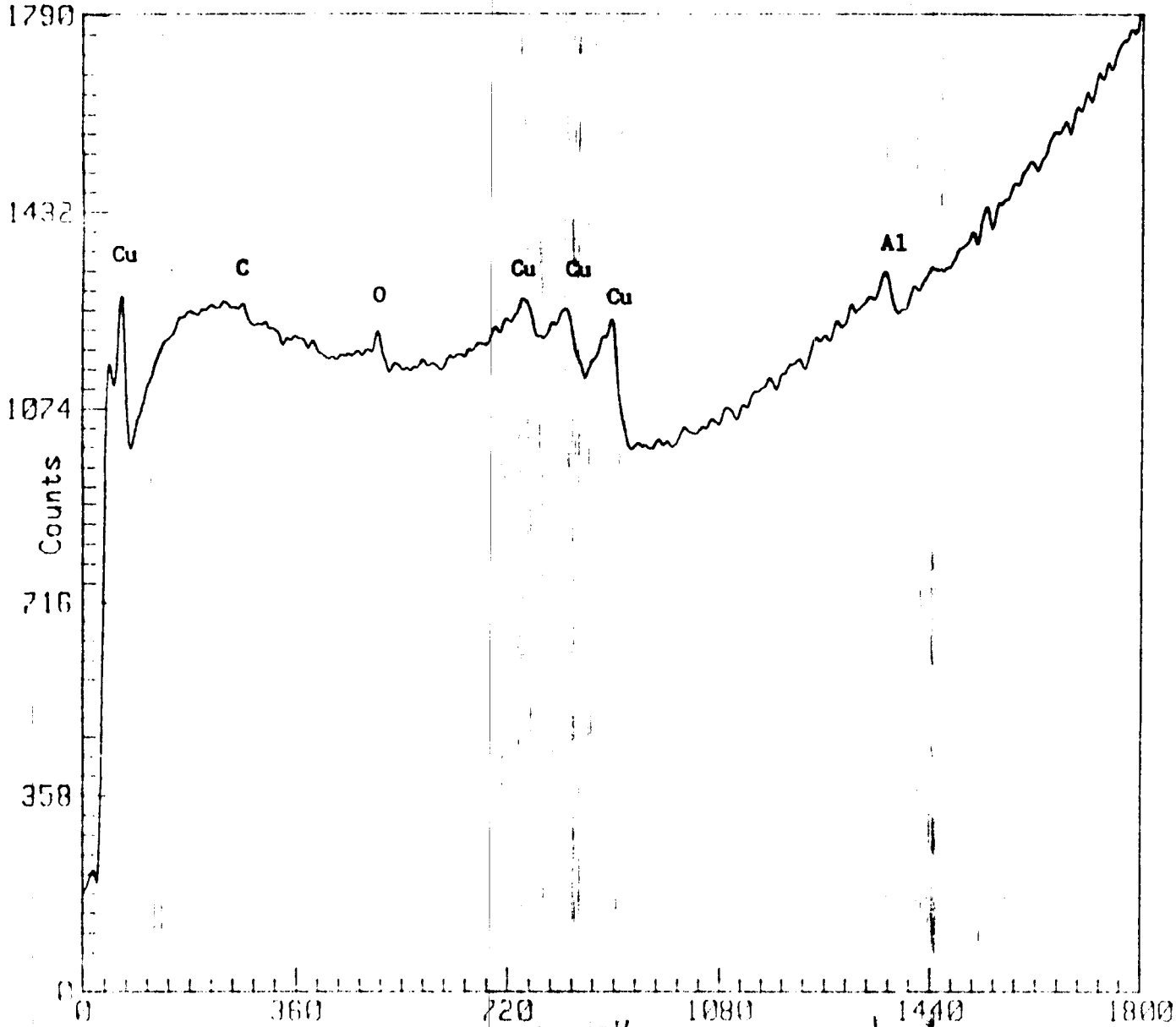

FIG 14

Spectrum of point C.

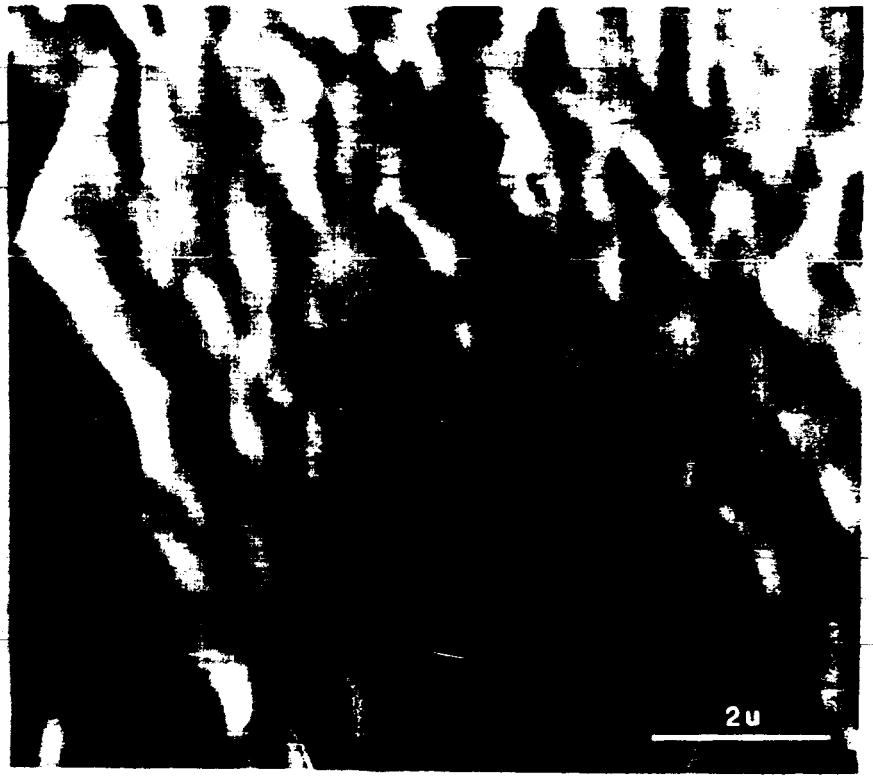

Al 'matrix', point F

FIG 15

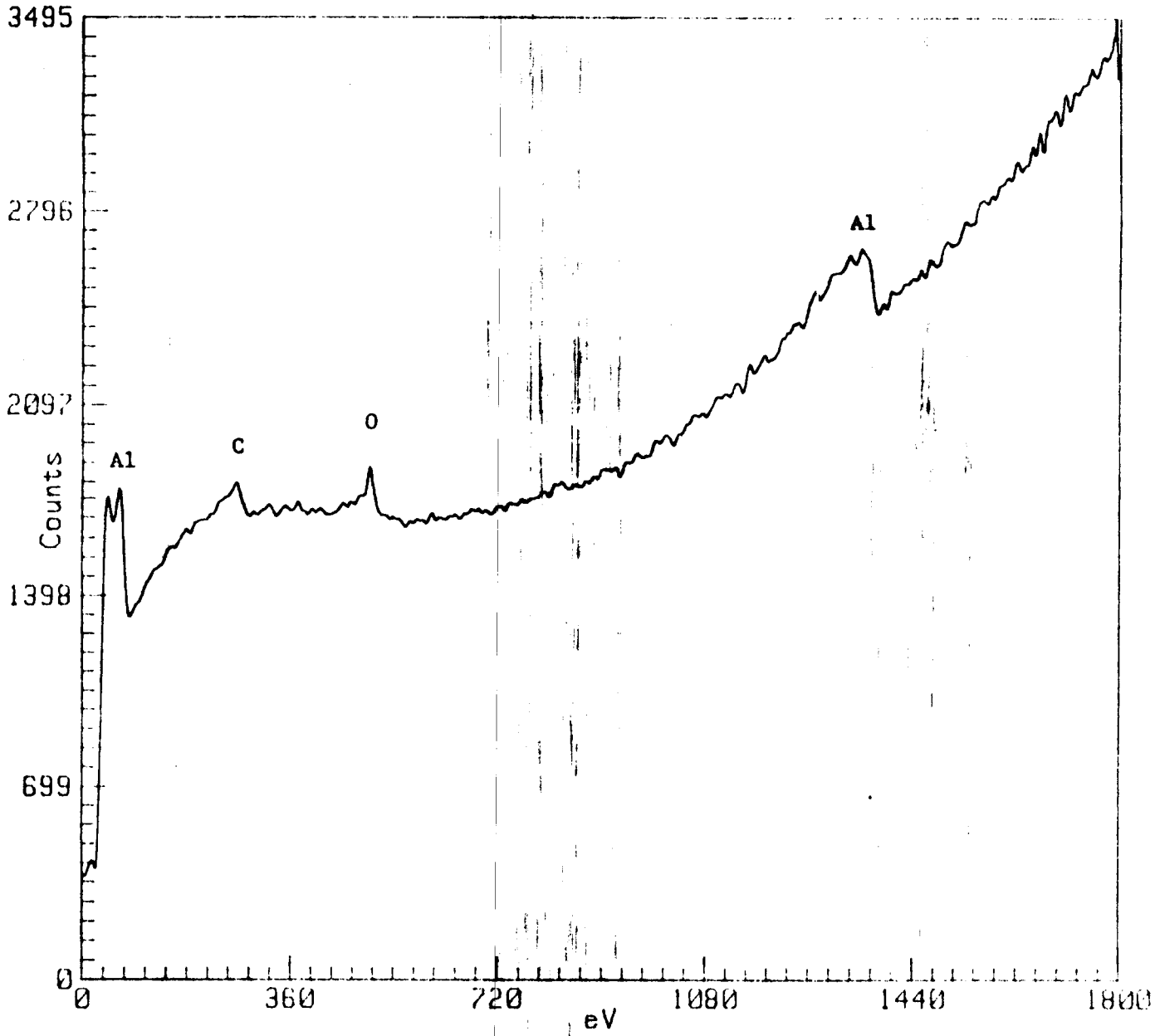

FIG 16

Al 'MATRIX', point f

FROM:

R.Browning

NASA-Ames Research Center

Mail stop 230/3

Moffet Field

CA 94035

TO:

Bill Brewer, NASA Langley

25 Nov 84

Dear Bill,

This is an informal report of our work on your SiC in Al2124 specimens. I will let you judge from the results whether to produce a formal report or paper and what to put into it. I would anyway in the case of a formal report want to include your observations and comments to interpret what is happening. I am writing a paper on one of the purely technical microscopy problems involved in analysing such systems. I will let you have this as soon as it completed as it will give you some more background to these results.

The three specimens studied were all the 0.05in. hot rolled specimens you sent me.

1) STND: Al2124 hot rolled to 0.05in. thick with T6 temper.

2) T6.05: SiC in Al2124 hot rolled to 0.05in. thick with T6 temper

3) F.05: SiC in Al2124 hot rolled to 0.05in. thick as extruded

The preparation of the specimens and the experimental conditions are covered in appendix A.

The results of the investigation were not at all what we expected to find, or what we were looking for at the start of the project. So I think it would be useful to summarize the negative results first and go onto the results that perhaps are more meaningful.

The major negative result is that no reaction zones between the SiC and the alloy matrix were found. The spatial resolution of the Auger technique equals the resolution of the beam 0.1u. So this means that if any reaction products remain in contact around the SiC then they are formed into a zone of less than this thickness. Further experiments to determine whether the remnants of a reaction zone still adhered to the SiC wiskers after polishing were also negative. As the Auger technique samples only 6-20 A, a very thin layer, a strongly adherent reaction zone might be expected to be seen on top of some of the SiC wisker surfaces. No real evidence was found to suggest that any SiC

wiskers had adherent reaction zones greater than 0.2u. However because of the finite resolution of the beam, the high noise in the measurement, and the small size and irregular topography of the wiskers I cannot say there are no adherent reaction products. They are just very unlikely. The limit of the resolution and stability of the microscope was reached in these experiments for spectra so a statistical method was tried. As the size variation and random distribution of the wiskers would be expected to give some exposed areas of a reaction zone, and if these areas were greater than 0.1u we might see them. However a statistical method based on the close association of SiC and Mn Fe and Cu did not succeed in producing any positive result.

The second major negative result was that there was no observable difference between the as extruded specimen F.05 and the artificially aged specimen T6.05

With what we didn't find out of the way I will start on what we did find. It is interesting to note that the major conclusion of this study was contained in the results of the last report I sent you (Sept83). I had overlooked it until now.

From our phone call of 19 April you pointed out that there are two intermetallic Al precipitate phases we would expect to see. Both precipitates contain Cu one phase with Fe and the other with Mn. In the standard alloy without SiC (STND)

this is pretty well exactly what we see. See appendix C for the experimental results on this specimen. In contrast to this, the intermetallics we see in the alloys with SiC are Cu/Al and Mn/Fe/Si/Al. This is our major result. No measureable trace of Fe is present in the Cu/Al phases found in the SiC/Al2124 specimens . Appendix D points out the comparison in the spectra between the Cu/Fe/Al of the STND alloy with the Cu/Al of the SiC/Al2124 specimens. No other intermetallic phases appeared to be present in the SiC/Al2124 specimens ie Al/C ect, But these may well have been missed in the general complexity of the alloy/wisker system. There is definitely a problem with these complex systems of identification of small areas. There are so many small features to investigate to find a precipitate with a total area of say 0.1% means testing hundreds of small features and completeness of analysis cannot be guaranteed.

Auger imaging of the SiC/Al2124 samples was undertaken to find the reaction zones but this instead showed that the two intermetallic precipitates were losely associated with the SiC wiskers. The association while not strong is clear. In some cases small intermetallics were observed decorating the larger SiC wiskers, often near the ends or sharp regions of the wiskers. In other cases larger intermetallic precipitates were found in close proximity to one or more SiC wiskers or between them. Areas that were free of SiC were also relatively sparse in precipitates. Several multiple Auger images were taken to test this and these are shown in

appendix B the results from T6.05.

So where are we now ? We have different precipitates in the SiC/Al2124 and the standard alloy. We have no reaction zones but there is some spatial correspondance beween the anomalous Si/Fe bearing precipitates and the SiC wiskers in the reinforced alloy.

Here I will indulge in some speculation

Would we be expected to see reaction zones anyway in the much rolled SiC/Alloy specimens? Well not perfect ones but we would expect to see the reaction products show up. Perhaps not at the SiC interfaces but near. Would we then expect to see different interface effects between the F.05 and the T6.05 specimens? Perhaps not if the reaction is is largly over beween the reactants and the SiC whiskers during formation and rolling.

The experimental conclusions are these:

* The addition of SiC to the Al2124 alloy changes the intermetallic precipitation behavour

*Two intermetallic phases have been found in the SiC/Al2124 system. One intermetallic contains Cu and Al and therefore is most likely CuAl2. The other intermetallic contains MnFeSiAl.

*No carbide phases were found, but the completeness of the anslysis is suspect.

*No reaction products were found adhereing to any SiC whiskers.

*There is a clear but not strong spatial association of intermetallic precipitation with the SiC.

*The T6 temper and the F as extruded SiC/Al2124 systems were indistinguisable in these experiments.

With these conclusions I will make the following suppositions:

*If there is no free Si in the SiC then the SiC reacts with the 2124 alloy to form MnFeSiAl. The carbide products have been missed or are too small for the microprobe.

*If any reaction products are formed at the SiC to alloy interface, then they are dispersed by the effects of hot rolling, both mechanical and diffusive.

*The reaction products if any, are not tightly bound to the SiC and may well be mobile.

* The major interaction beween the SiC and the Al2124 has been completed before aging, but a reaction during aging is

therefore a posibility.

If these conclusions and suppositions have some validity then there are two dependent questions that could be posed

1) Are these conclusions important.

2) Is it possible to make a model system to follow the reaction more accurately, ie large wiskers not rolled.

APPENDIX A.

Specimen preparation and experimental conditions.

All three specimens were washed in alcohol for degreasing. The specimens were cleaned in UHV using 3keV Argon ions with a total cleaning time equivalent to approximately 100Å removed.

A 5keV, 3nA beam of 0.1u size was used for the majority of the experiments. The CMA resolution used was 1%.

APPENDIX B.

Results on T6.05, SiC in Al2124 with T6 temper.

Fig B1 shows a low magnification SEM image of a general specimen region, Mag 1K.

Several different regions could be identified from their SEM contrast. SiC and Al and Mg oxides were most clear. The two intermetallic phases that were found were of similar contrast and slightly lighter than the matrix. The intermetallics were of two distinct types and generally formed in well separated regions of up to 20u in size. The spectrum from the MnFeSiAl region is shown in fig B2. Further spectra from these two regions are presented in appendix D, the results from Specimen F.05. The spectrum fig B2 shows the overlap with the Mn and Fe peaks. It can be seen that two of the three Mn and Fe peaks overlap. With the noise in the measurement the Fe was origonally overlooked. From the results on this specimen and the results on the F.05 specimen it can be clearly seen that the Fe has preferentially precipitated with the Mn and Si.This is dicussed more fully in appendix D.

The two precipitate phases that were found appeared to be associated with the SiC fibers and a new technique was invented to confirm and display this association. The technique of multi-spectra false color imaging allows the MnFeSiAl, the CuAl2 and the SiC to be imaged similtaneously in separate colors. Brown for SiC, purple for MnFeSiAl,

and,naturally, green for Cu Al. Although the images in certain areas appear noisy, just single pixels appearing, Where the pixels are green or purple these are generally significant. In a large area scan of the SEM fig B1 it was found that the areas of the precipitates were CuAl-4%, MnFeSiAl-1% with SiC being 20% of the area. This is just an indication of the areas and not strictly planimetric. There are several problems involved in this measurement. Some of which will be covered in a later paper.

Several false color images were taken over the area seen in the SEM fig B3. This is the region seen in the mid upper right in SEM fig B1. This is where there is a region free of SiC wiskers. Figs B4 to B17 are false color images from this region, the specific sites are indicated in a grid in fig B3. The association of the precipitates with the SiC can be seen from these figs. For example in fig B7 there is little SiC and very little pecipitate. Alternatively the large CuAl and MnFeSiAl regions are associated with clumps of SiC see figs B10,B12. In some experiments the precipitates were found associated inbetween two close SiC fibes or near the sharp ends of fibers, but not in all cases.

Fig B2

Mn Fe Si Al

T6.05
SiC/Al2124

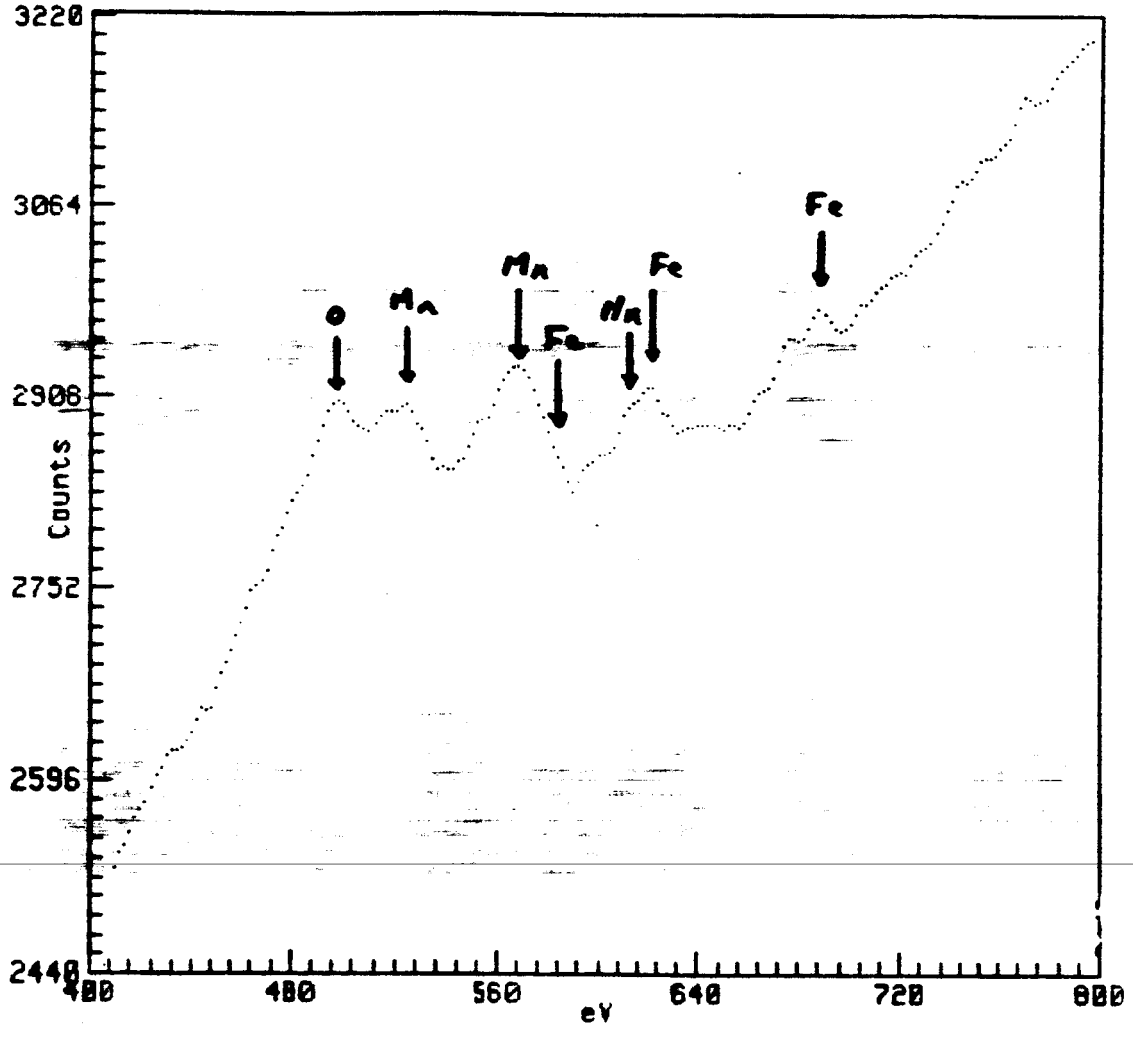

APPENDIX C.

Results on STND, Alloy Al2124 with T6 temper.

Fig C1 shows an SEM from one area on this sample that showed some larger precipitate areas. These areas were identified by their slightly different topographical relief. The large precipitates were found to be complex and composed of two areas. Spectra from the two areas are shown in fig C2. These phase areas were found to be the expected precipitates CuFeAl and CuMnAl. The CuFeAl phase spectrum A is the upper line of fig C2 and the CuMnAl phase spectrum B the lower. The precipitate areas were imaged using false color imaging fig C3. The pixel step in fig C3 is 1.2u but the resolution of the beam is 0.1u. The image is 150u across. Fig C3 shows there is a wide distribution of precipitate sizes and the large precipitates are finely mixed regions of the two phases CuFeAl and CuMnAl. The CuFeAl has been imaged in green, the CuMnAl in purple and the ochre pixels are the overlap betwwen the two precipitates. Only two precipitates are believed to exist. There are only 25 noise pixels in this image. That means the single, double and small multiple pixel groups are significant and not noise.

Because of the fine spatial mixing of the precipitates there is some problem in getting a spectrum from just one region. But it does appear from a compilation of many spectra that the CuMnAl phase may well have a small amount of Fe.

Fig C4 is an expanded spectrum from the CuFeAl phase and can be compared with the same region in the CuAl2 phase of the results in appendix D.

Fig C4

Cu Fe AL

STND
AL2124

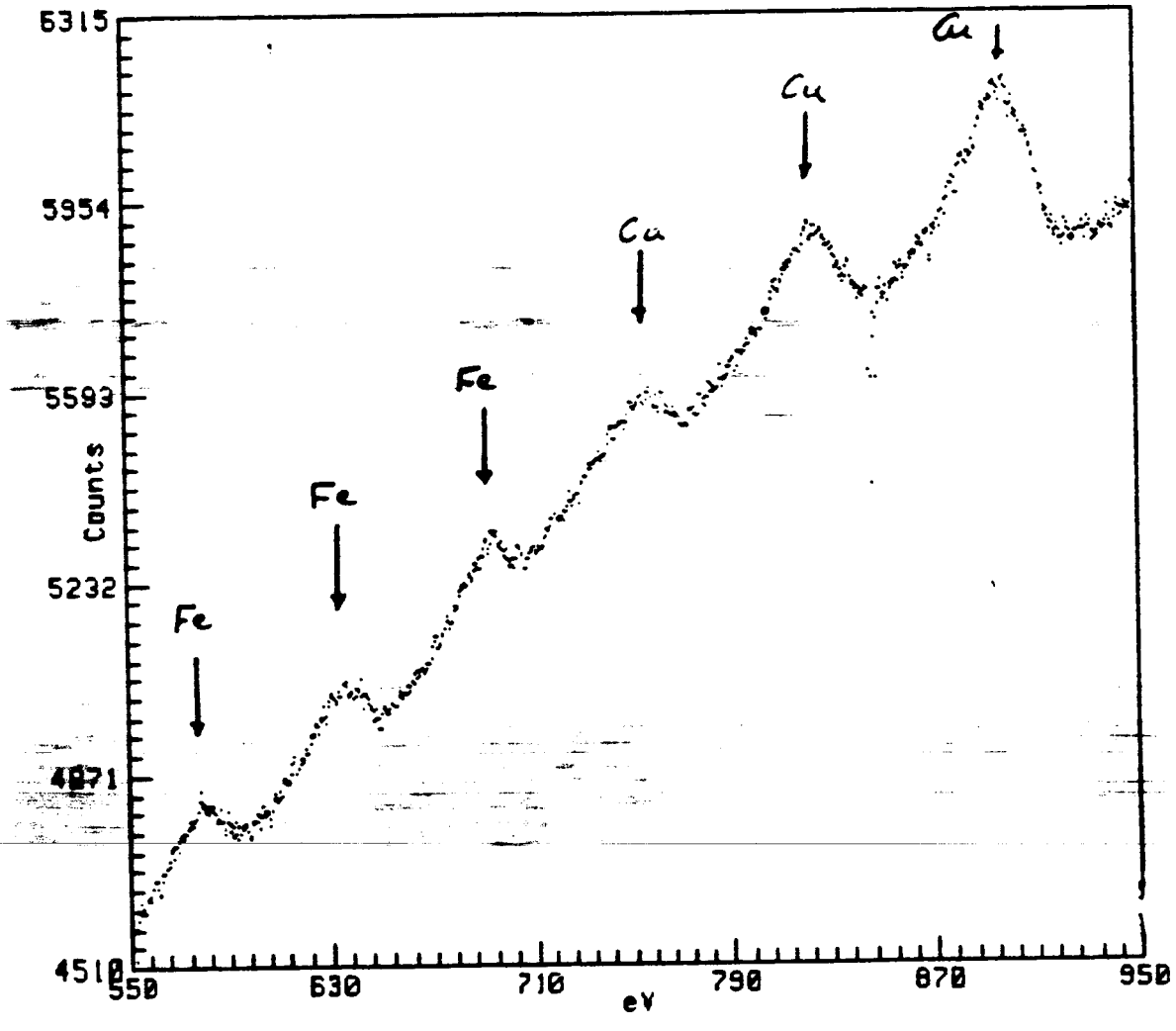

APPENDIx D.

Results on F.05, SiC in Alloy Al2124 as extruded.

Fig D1 shows an SEM from one area on this sample. The overlay indicates the composition of the features. The spectra from the SiC and the precipitate regions are shown in figs D2,D3,D4. In fig D2 the SiC spectrum shows the distinct features of the Si and C Auger transitions at 90eV and 260eV respectively. In fig D3 the Cu and Al features can be seen clearly. Here the C and O are probably just surface contamination. In fig D4 the MnFeSiAl phase shows up well.Comparison of the Si peak height in this fig with the Si in the SiC shows that the Si content is considerable. Again the C and O are probably surface contaminants. Compare the CuAl phase fig D3 with the spectrum from the STND CuFeAl in fig C4. There is clearly little if any Fe associated with the CuAl2.

Fig D2

SiC.

F.05

SiC/AL2124

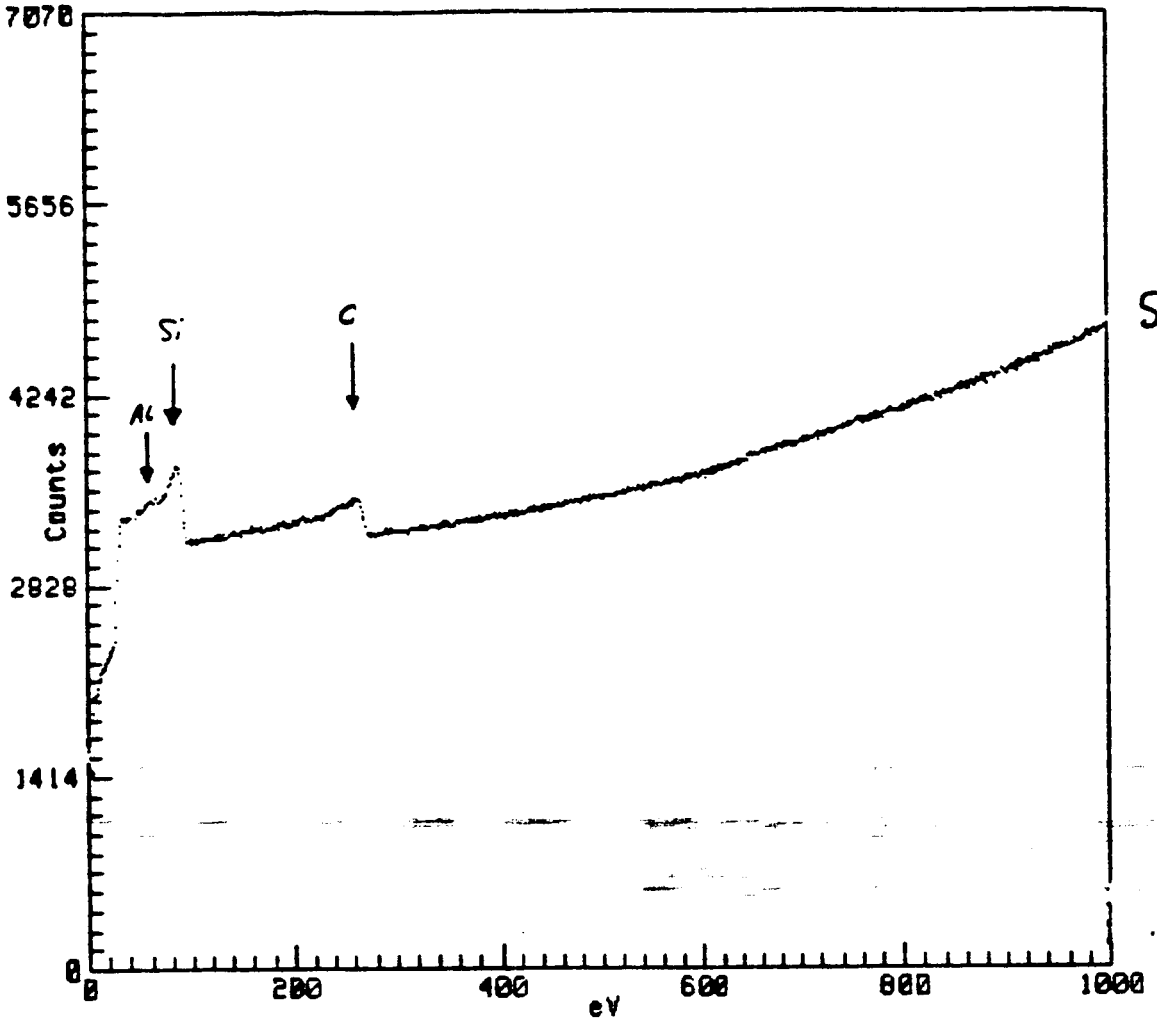

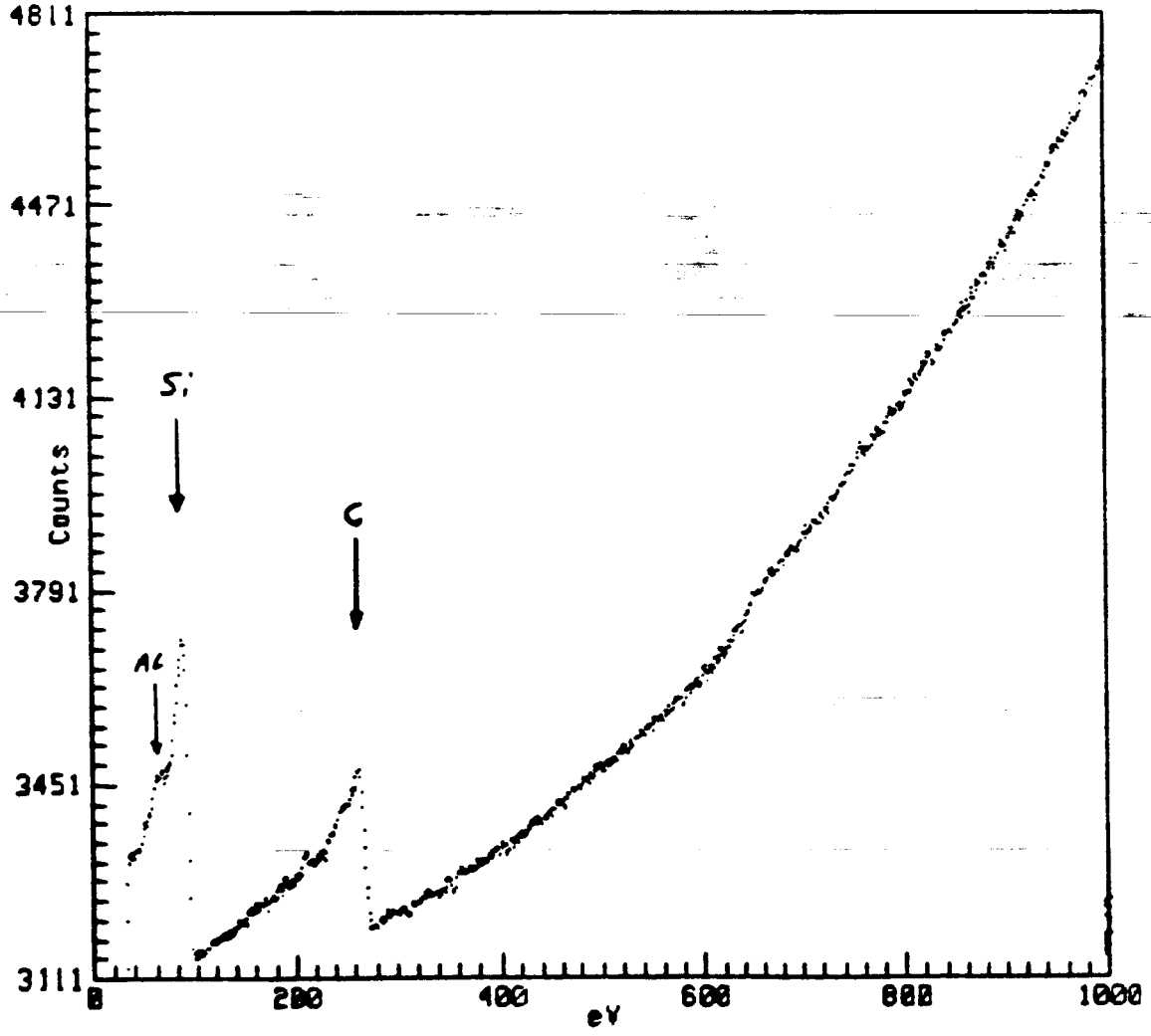

Fig D3

$CuAl_2$

F.05

SiC/Al2124

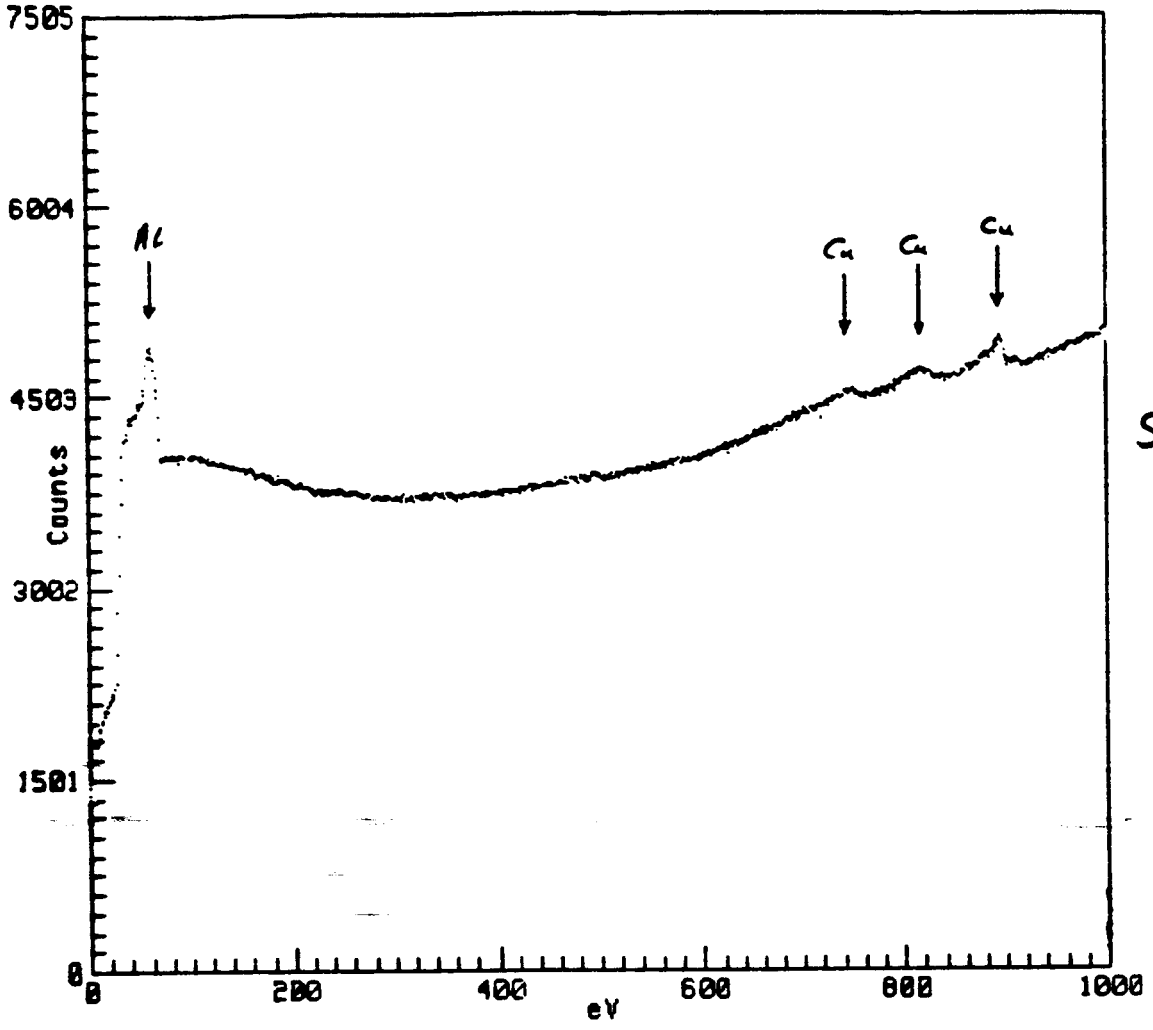

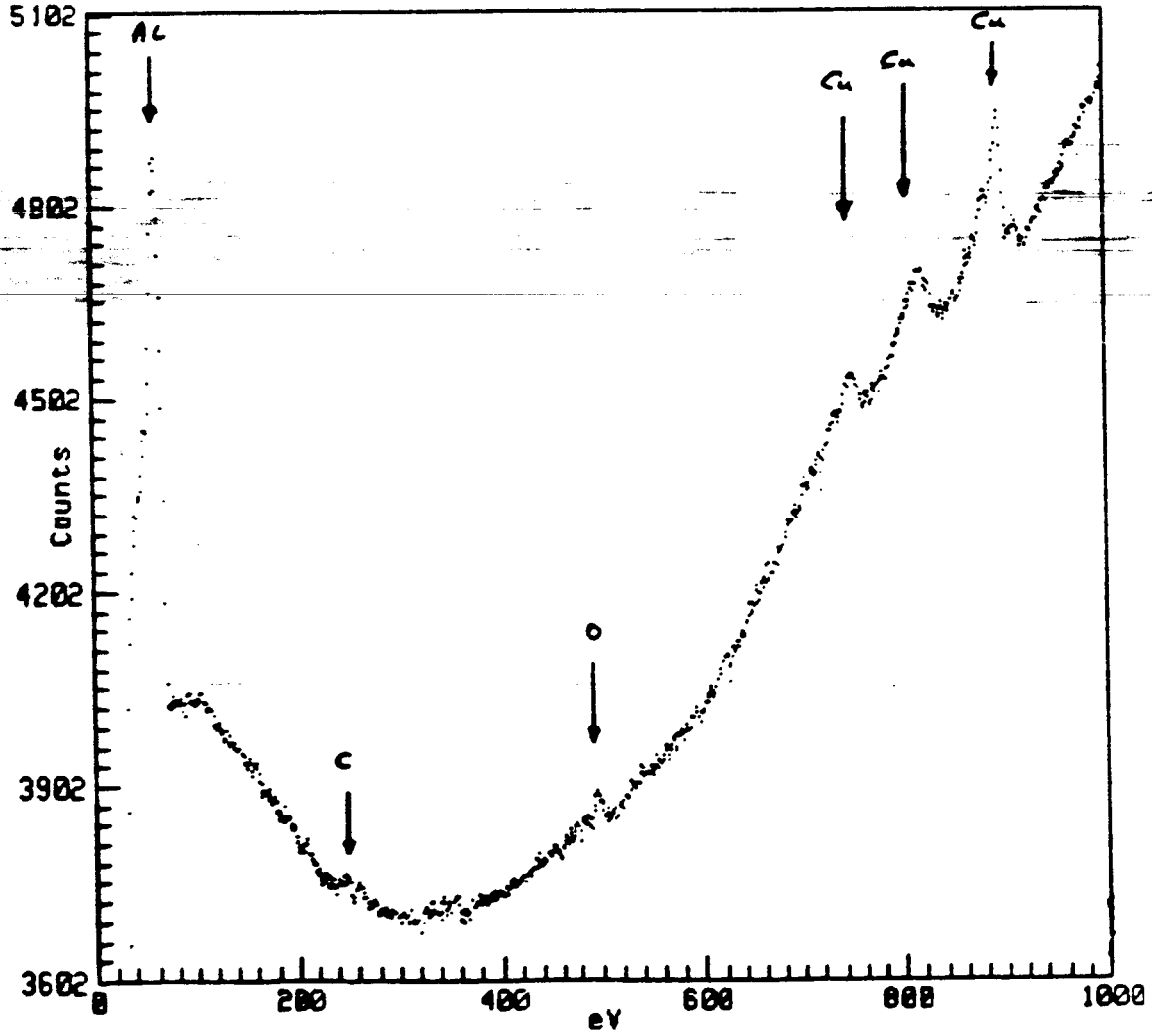

Fig D4

Mn Fe Si Al

F. 05

SiC/Al2124

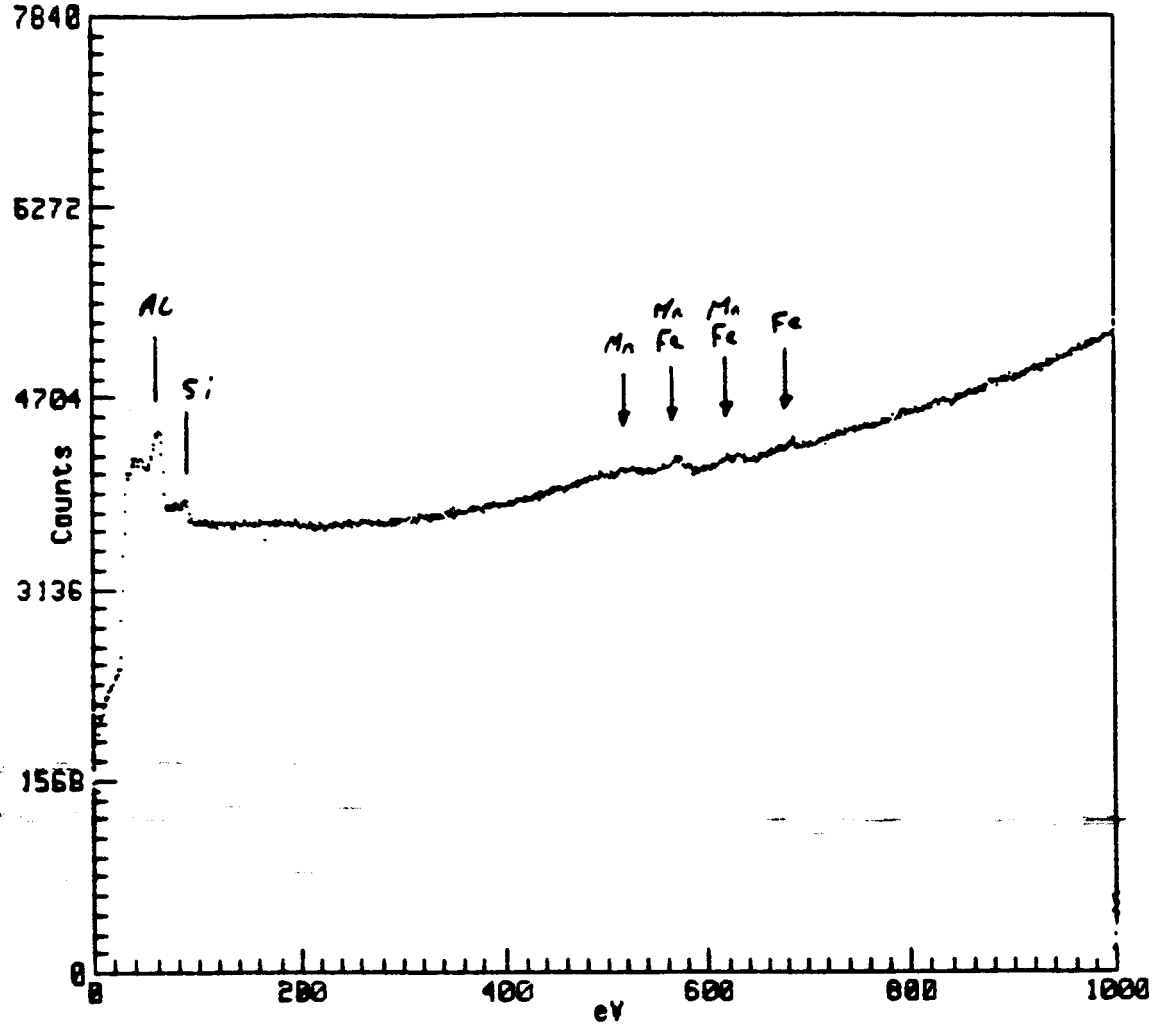

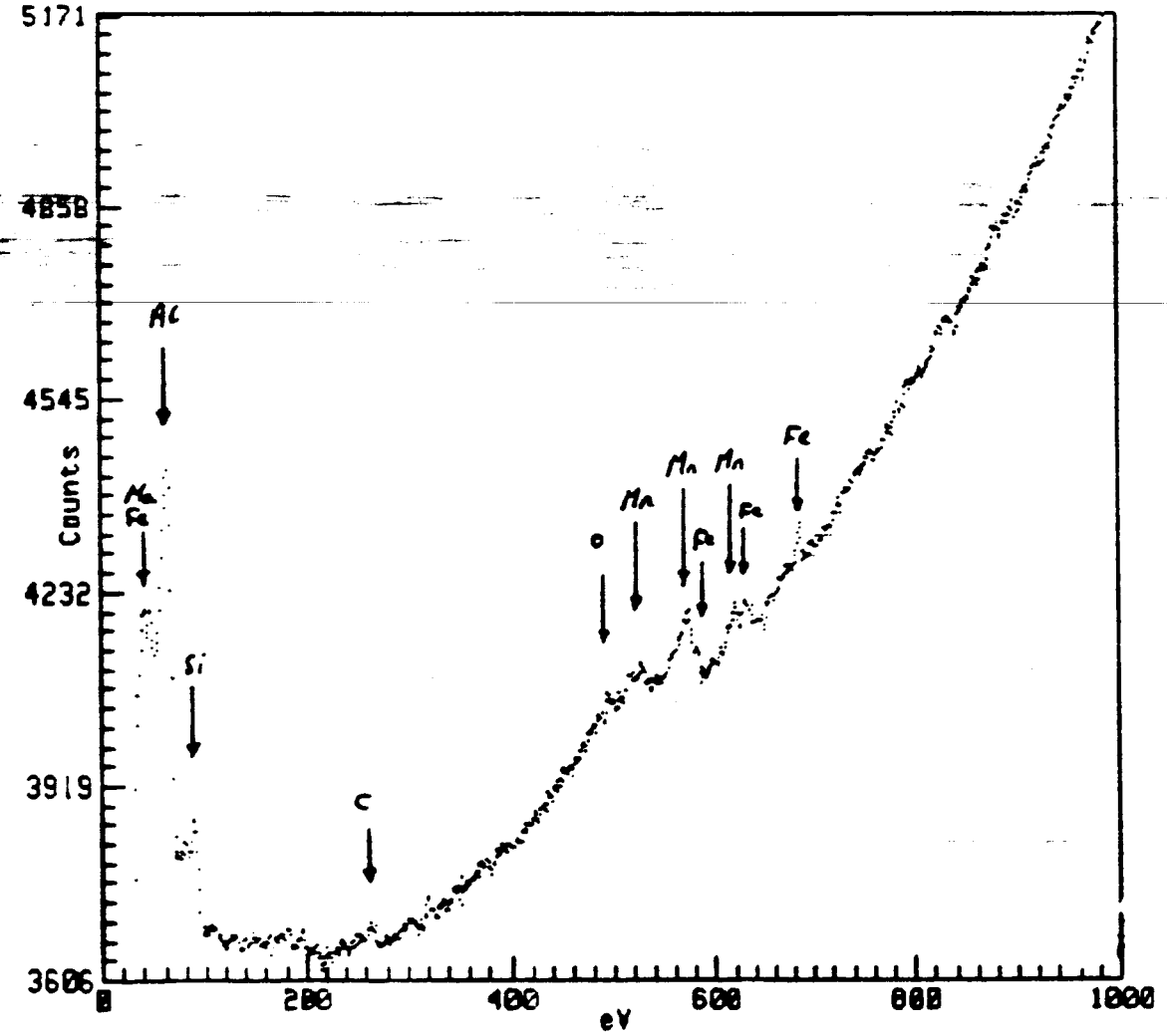

ref 11

Interfacial layers in high-temperature-oxidized NiCrAl

L. A. Larson, R. Browning, and H. Poppa
NASA Ames Research Center, Moffett Field, California 94035

J. Smialek
NASA Lewis Research Center, Cleveland, Ohio 44135

(Received 24 September 1982; accepted 17 November 1982)

The oxide and diffusion layers produced in a Ni–14Cr–24Al alloy by oxidation in air at 1180 °C for 25 h have been studied using scanning Auger microscopy and ball cratering for depth profiling. During cooling, following oxidation, the oxide layers formed by this alloy spalled profusely. The remaining oxide was very thin (< 100 Å) and was primarily Cr_2O_3 with a trace of Ni (although other oxides are possible). The underlaying metal substrate exhibited γ/γ' (Ni/Ni_3Al) and β (NiAl) phases; however, there was metallic interfacial layer at the surface. This layer was similar to the bulk γ/γ' phase, but slightly enriched in Cr and Al. These data are compared to electron microprobe results from a nominally identical alloy. The diffusion layer thickness is modeled with a simple mass balance equation and compared to recent results on the diffusion process in NiCrAl alloys.

PACS numbers: 81.60.Bn, 82.80.Pv, 68.60.+q, 79.20.Fv

I. INTRODUCTION

The high-temperature oxidation resistance of MCrAl alloys is the result of their ability to selectively oxidize Al to Al_2O_3. The high-temperature oxide phase α-Al_2O_3 allows minimal oxygen diffusion, thereby providing protection between the metal and the environment.

It is generally agreed that the kinetics of formation of this α-Al_2O_3 layer involves primarily the inward diffusion of oxygen, with the outward diffusion of Al, resulting in the formation of Al_2O_3 at the oxide–metal interface.[1] An O^{18} tracer study has shown that the rate-controlling parameter for Al_2O_3 formation is the inward oxygen diffusion via grain boundary transport.[2] However, an examination of transport properties of the constituents of the alloy reveals that the ability of the metal to provide the necessary Al flux is vital to the composition of the oxide layer.[3] Alloys with low Al concentration (4%–6%) do not develop sufficient Al flux from the metal to form the protective Al_2O_3 layer; instead, the less protective oxides of the other alloying metals form. These oxides allow further diffusion of oxygen into the alloy resulting in internal Al_2O_3 precipitates.

The aluminium diffusion processes are particularly important for superalloy overlayer coatings. In this case, aluminum diffusion from the coating into the substrate metal has been observed.[4,5] If the diffusivity of Al into the substrate is high, more Al may be lost to the substrate than is used in oxide overlayer development. As this reservoir is depleted, the coating may not be able to supply sufficient Al for Al_2O_3 formation, and the coating will not provide oxidation protection.

Diffusion of Al to the oxide–metal interface implies the depletion of Al in the bulk metal. This takes place in the form of a depletion zone in the near-surface region metal.[3] This is apparent in metallographical sections after severe exposures.[6] It is the purpose of this paper to point out this diffusion zone, the attendant changes in composition, and the utility of Auger electron spectroscopy combined with ball cratering for this type of depth analysis.

II. EXPERIMENTAL

Buttons were made from Ni 270 sheet, iodide Cr, and Al shot (all 99.99% pure) by melting in a tungsten electrode arc. Samples approximately 5×5×1 mm thick were cut by a diamond wafering wheel. After annealing in Ar for 24 h at 1100 °C, they were metallographically polished and cleaned. Oxidation in air was carried out at 1180 °C in an FeCrAlY specimen holder which had been preoxidized to form a thick Al_2O_3 film to avoid contamination of the surface. Following oxidation (during cooling to room temperature) the oxide spalled profusely. This Ni–14Cr–24Al (at.%) sample was ball-cratered in a spalled region through the remaining oxide deep into the base metal for Auger depth-profiling analysis. Ball-cratering is a method of polishing a spherical indentation into the sample. In this case, a 5/8 in. sphere was used with 1-μm diamond paste. The spherical section formed by the ball cratering was 2.2 mm in diameter and approximately 65 μm deep. Stylus profilometer measurements of the crater thus formed were in good agreement with the geometrical depth estimates. Following cratering treatment, the sample was transferred to the Auger microprobe for analysis.

The Auger observations were made using a 30-nm-diam beam of electrons with 5 kV energy in the microprobe described previously by Todd *et al.*[7] The microprobe was operated under computer control to obtain selected point spectra as well as scanning Auger micrographs with high lateral resolution. Overall surface contamination was removed by Ar ion bombardment at 3 kV and ~1 μA/cm^2.

III. RESULTS

An oblique view of the edge of the ball crater in the NiCrAl sample is shown in Fig. 1. The oxide surface formed

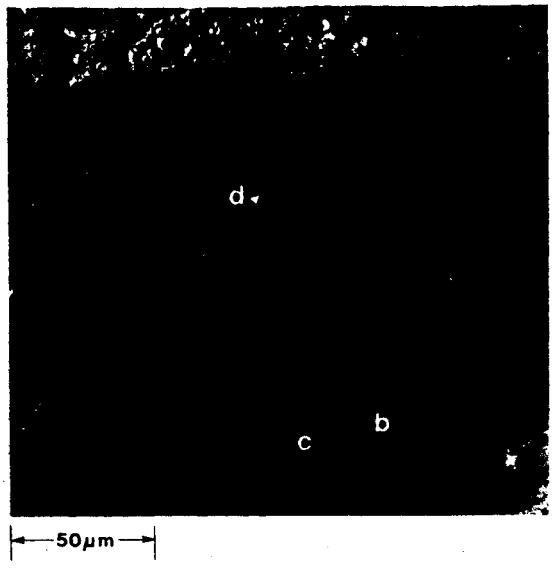

FIG 1. SEM image of the oxidation layers in the ball-cratered NiCrAl alloy. (a) Oxide surface, (b) γ/γ' phase bulk metal, (c) β phase bulk metal, and (d) interface zone (γ phase).

after spalling is labeled (a). Deep inside the crater, the γ/γ' and β phases of the bulk NiCrAl are visible as regions with slightly different contrast, these are labeled (b) and (c), respectively. The diffusion zone is the near-surface area in which no phases are distinguished, labeled (d).

A. Bulk phases

The compositions of the thermodynamic phases of the bulk NiCrAl alloy are well known[6,8] and are presented in Table I along with the results from this study. This is a two-phase alloy with roughly equal volumes of the γ/γ' and β phases. The γ/γ' phase is considered a matrix of the γ phase (Ni solid solution) with interspersed cubic γ' particles (Ni_3Al). The β phase is considered NiAl with interspersed α-Cr particles.[6] The γ' and α-Cr particles both have a characteristic dimension of approximately 500 Å, and thus are too small to be resolved in this study.[8]

TABLE I. Metal compositions (at. %).

		Ni	Cr	Al
Nominal		61.2	15.3	23.5
β phase	a	59.8	11.1	29.1
	b	58.2 ± 2.1	8.4 ± 1.0	33.3 ± 2.3
γ/γ' phase	a	62.9	22.1	15.0
	b	63.6 ± 1.5	22.0 ± 1.3	14.6 ± 1.6
Diffusion zone (γ phase)	b	59.5 ± 1.7	24.7 ± 0.6	15.6 ± 1.5

[a] Electron microprobe analysis of nominally identical samples, average of 50–100 spectra, from Ref. 8.
[b] This study.

The compositions obtained in this study are the averages of ~25 Auger spectra from each type of area. The individual spectra were analyzed using sensitivity factors obtained from elemental spectra taken on the same machine under identical conditions, then self-normalized and averaged as a group. The error reported is 1 rms deviation of that average. The results reported in Table I are in good agreement with the electron microprobe results listed in the same table. The deviations observed in the β phase compositions can easily arise from slightly different histories of nominally identical samples.

It should be noted that an appreciable carbon contamination (on the order of 10%) was observed on all metal surfaces in the form of a carbide-type peak. However, Musket *et al.* have observed in a review article that Ar ion cleaning is not sufficient to remove residual C from Ni- and Fe-based metals.[9] Furthermore, it has been shown in this laboratory that these C signals are a preparation artifact of the Ar ion cleaning.[10] The carbon signal was removed from the reported data as part of the normalization procedure.

B. Oxide layers

Pure NiCrAl forms a protective Al_2O_3 layer during oxidation. This particular alloy also spalls that oxide layer profusely during cooling. Oxidation rate data published by Kahn, Lowell, and Barrett[6] indicates that about 3.2 μm of Al_2O_3 should form during the 25 h oxidation. Islands of Al_2O_3 of approximately that thickness were observed scattered over the sample. The general oxide left in the spalled areas was a mixture of Cr and Ni oxides. A representative Auger spectrum of this residual oxide is shown in Fig. 2. This oxide was very thin; it was removed within 30 min of Ar ion cleaning (~1 μA/cm², 3 kV). Analysis of a limited number of Auger spectra indicated that the composition is Ni = 11.4 ± 3.0%, Cr = 33.4 ± 1.3%, and O = 55.2 ± 2.3%. The best fit to these data is 89% Cr_2O_3 with 11% metallic Ni. It is possible that these spectral data represent microscopic Cr_2O_3 islands with bare metal between, or perhaps cracks in a Cr_2O_3 layer. The shapes of the Ni peaks in Fig. 2 do not exhibit the loss features that

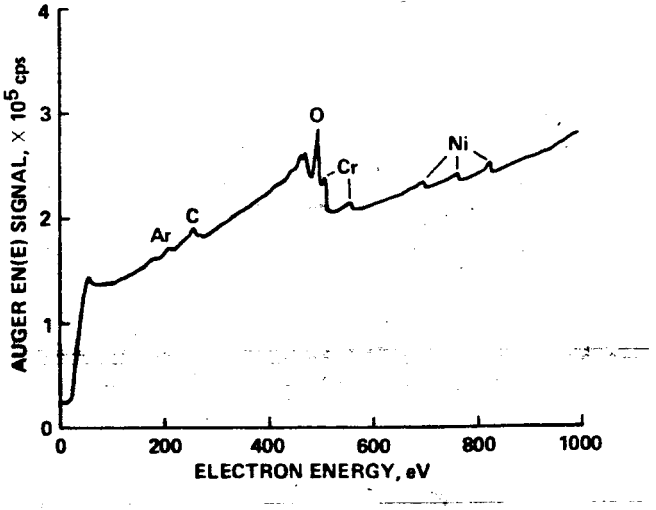

FIG 2. Auger $EN(E)$ spectrum of the oxide formed after spalling (primary energy 5 kV, beam current 10 nA).

would be expected from subsurface Ni.[11] Therefore, monolayer amounts of continuous Cr_2O_3 over the base metal are not as likely. Other oxides such as 80% $NiCr_2O_4$ + 20% Cr_2O_3 and 20% NiO + 80% Cr_2O_3 (all of which are known oxide species for this kind of alloy) are possible but do not fit the data as well.

C. Interface layer

As noted previously, the Al necessary for forming the Al_2O_3 layer is supplied by the base metal. This results in the formation of an Al depletion zone in the near-surface metal with respect to the nominal alloy. The compositional difference is also very clearly delineated in the chromium scanning Auger micrograph of Fig. 3 as the region with little contrast as compared to the bulk phases. A correlation between the micrographs and the known geometry of the ball crater indicates that the depth of this zone is 12.5 μm. The average composition of this zone is shown in Table I, in addition to the bulk phases. In comparison to the bulk γ/γ' phase, this layer is enriched in Cr but contains about the same Al. The most striking feature of this zone is the complete lack of β phase metal (light regions in Fig. 1, dark regions in Fig. 3). The interface between the bulk metal and the diffusion zone was found at a uniform depth around the circumference of the crater. Spectra taken near the β phase/diffusion zone interface were consistent with the average values for the particular metal. Similarly, no diffusion gradients in composition were observed to within approximately 3% error. The uniform composition observed for this interface is indicative that γ phase metal has been formed[6] from the decomposition of the nominal γ/γ'–β alloy.

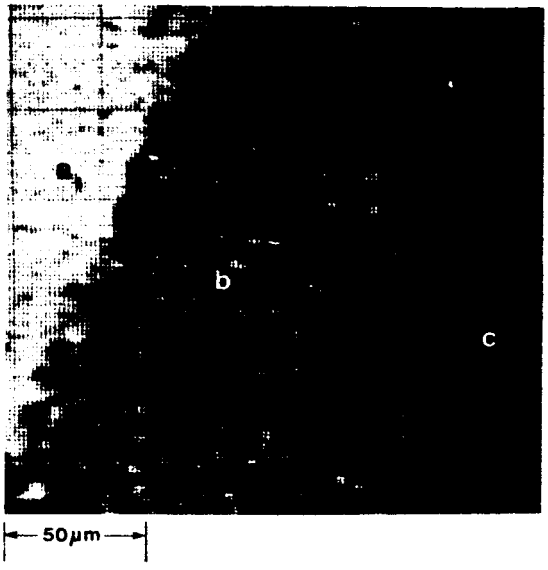

FIG 3. Chromium Auger image of the crater edge. (a) Oxide surface, (b) interface layer, and (c) bulk phases.

IV. DISCUSSION

We have observed that the residual oxide on the NiCrAl following oxidation is primarily Cr_2O_3 with a few islands of Al_2O_3 that had not spalled. However, [illegible] oxidation this NiCrAl alloy [illegible] Al_2O_3-Cr_2O_3 formation in this alloy is [illegible] temperatures and in transient oxides. These observations combined with the thinness (<100 Å) of the Cr_2O_3 imply that the spalling occurred primarily during cool down.

A relatively simple model can be proposed which describes the diffusion/oxidation results for this sample. Interpolation of the data from Kahn, Lowell, and Barrett[6] leads to an Al_2O_3 thickness of 3.8 μm (from a parabolic scaling constant of $k_p = 0.02\ mg^2cm^{-4}h^{-1}$) formed during the 25-h oxidation at 1180 °C. A mass balance equation can be written requiring the initial bulk metal (Auger data) to form Al_2O_3 and the observed γ phase interface metal. Solving the equations for the Al and Cr constituents leads to the prediction that the interface is 12.5 μm in depth, which is in excellent agreement with the observed 12.5 μm depth. Using the nominal composition of the original alloy leads to an interface thickness of 13.1 μm which is comparable to the observed value. Implicit in this calculation is the assumption that the Cr content of the original metal is retained in the γ phase interfacial region. The Ni component of the original metal does not balance with that retained in the interfacial zone. As a significant amount of Ni oxide is not observed during the oxidation process, it is implied that the bulk metal serves as a sink for the back diffusion of Ni during oxidation. However, the corresponding Ni accumulation in the bulk was not observed.

A study of solute transport during the cyclic oxidation of NiCrAl alloys has been recently reported by Nesbitt.[3] In this work, diffusion coefficients were experimentally determined for Zr-doped NiCrAl alloys. These results were then utilized in a numerical model to predict γ layer thickness, the concentration/distance profiles, and the weight of Al consumed. Quantitative energy-dispersive x-ray spectroscopy confirmed the results of the calculations. There is excellent agreement between Nesbitt's calculations and the results reported here. The concentration/distance profiles show clear Al and Cr transport toward the oxide/γ phase interface while Ni diffuses toward the bulk. For short times (under 100-h oxidation) the gradients through the γ phase interface zone are shown to be less than 2% which is inside the error expected in this work.

One example of isothermal oxidation (used in this work) was given in Nesbitt's[3] report. His results from this sampling support the comparative differences between these works. These differences are a significantly smaller γ phase interface width, minimal diffusion gradients, and a slight increase of the Al concentration of the interface metal for isothermally oxidized samples in comparison to cyclic oxidation. All of these effects are due to the oxide spalling that occurs during cyclic oxidation. Spalling of the protective Al_2O_3 layer leads to an increase of the average oxidation rate as a new protective layer is formed. This necessarily increases the demand for Al, resulting in increased γ layer widths, and larger diffusion gradients. For isothermal oxidation of up to 1000 h, Nesbitt found a significant decrease in γ layer width in comparison to cyclically oxidized samples, and nearly flat diffusion gradients in the γ phase interface layer.

V. CONCLUSIONS

The utility of Auger electron spectroscopy combined with ball cratering for depth analysis has been demonstrated. It should be noted that systems with less spatial resolution could be equally effective for the analysis of diffusion layers through utilization of this technique.

The agreement between the Auger results and published data from electron microprobe analysis is good and supports the effectiveness of AES as a quantitative analysis technique. In addition, a very thin Cr rich scale was observed that formed after the Al_2O_3 spalled off at some intermediate temperature during cooling.

ACKNOWLEDGMENT

Funds for the support of this study have been allocated by NASA Ames Research Center, Moffett Field, California, under Contracts NCC 2-176 and NAS 2-10987.

[1]F. A. Golightly, F. H. Stott, and G. C. Wood, Oxid. Met. **10**, 163 (1976).
[2]K. P. R. Reddy, J. L. Smialek, and A. R. Cooper, Oxid. Met. **17**, 429 (1982).
[3]J. A. Nesbitt, NASA Contractor Report 165544; also M. S. thesis, Michigan Technological University, 1982.
[4]J. L. Smialek and C. E. Lowell, J. Electrochem. Soc. **124**, 800 (1974).
[5]S. R. Levine, Metall. Trans. **94**, 1237 (1978).
[6]A. S. Kahn, C. E. Lowell, and C. A. Barrett, J. Electrochem. Soc. **127**, 670 (1980).
[7]G. Todd, H. Poppa, and L. H. Veneklasen, Thin Solid Films **57**, 213 (1979).
[8]J. L. Smialek and R. Gibala, Metall. Trans. (to be published).
[9]R. G. Musket, W. McLean, C. A. Colmenares, D. M. Makowiecki, and W. G. Siekhaus, Appl. Surf. Sci. **10**, 143 (1982).
[10]R. Browning and L. A. Larson (to be published).
[11]Y. E. Strausser, D. Franklin, and P. Courtney, Thin Solid Films **84**, 145 (1981).